

Calorimetric Measurements with Extremely Fine Spatial Resolution

Burak Bilki, Benjamin Freund and José Repond
On behalf of the CALICE Collaboration

Abstract—In special tests, the active layers of the CALICE Digital Hadron Calorimeter prototype, the DHCAL, were exposed to low energy particle beams, without being interleaved by absorber plates. The thickness of each layer corresponded approximately to 0.29 radiation lengths or 0.034 nuclear interaction lengths, defined mostly by the copper and steel skins of the detector cassettes. With its extremely fine segmentation of the readout based on $1 \times 1 \text{ cm}^2$ pads, the DHCAL provides unprecedented details of both electromagnetic and hadronic showers. This paper reports on measurements performed with this device in the Fermilab test beam with positrons in the energy range of 1 to 10 GeV. The measurements are compared to simulations based on GEANT4 and a standalone program to emulate the detailed response of the active elements.

I. INTRODUCTION

The major future colliders envisaged are the International Linear Collider (ILC) [1], Compact Linear Collider (CLIC) [2] and Future Circular Collider (FCC) [3]. The research on developing the highest precision detectors for these colliders to record the data of lepton-lepton, hadron-hadron or lepton-hadron collisions at unprecedented high energies is well underway. The major task for these experiments is to measure all the emerging particles at the collision with highest precision. As an example, the measurement of hadronic jets will play an important role in discovering or exploring physics beyond the current Standard Model of Particle Physics. Indeed, both the energy resolution and the mass resolution of multi-jet systems will be important in defining the physics reach of these new facilities. Of particular interest will be the identification of electroweak bosons through their hadronic decay. Identification on an event-by-event basis will require an energy resolution of the order of 3-4 % for a wide range of jet energies.

The High Energy Physics community has come to a consensus that the achievement of the high precision aimed in these experiments can be made possible with the utilization of the Particle Flow Algorithms (PFAs) [4]. PFAs attempt to measure each particle in a jet individually, using the component providing the best energy/momentum resolution. In this approach, charged particles are measured with a high-precision tracker, photons with the electromagnetic calorimeter and the remaining neutral hadronic particles in a jet with the

TABLE I

PARTICLES IN A JET, THEIR AVERAGE FRACTION OF THE ENERGY OF A GIVEN JET AND THEIR CONTRIBUTION TO THE OVERALL RESOLUTION.

Particle	Average fraction of jet energy [%]	Measured with	Contribution to resolution [σ^2]
Charged	65	Tracker	Negligible
Photons	25	ECAL with $15\%/\sqrt{E}$	$0.07^2 E_{jet}$
Neutral hadrons	10	Calorimeter with $50\%/\sqrt{E}$	$0.16^2 E_{jet}$
TOTAL	100		$0.18^2 E_{jet}$

combined electromagnetic and hadronic calorimeters. Table I shows the average fraction of the jet energy carried by these particle types and the expected single particle resolution obtained with the appropriate detector subsystem.

A detector optimized for the implementation of PFAs requires an excellent tracker within a high magnetic field, a large inner radius of the calorimeter (to increase the distance between showers from different particles), the calorimeters to be placed inside the coil (to avoid energy losses in the inert material of the solenoid), calorimeters with extremely fine segmentation of the readout (to separate showers from charged and neutral particles), an electromagnetic calorimeter with a short Molière radius (to reduce the lateral spread of electromagnetic showers) and a hadronic calorimeter with a short interaction length (to be able to place it inside the smallest possible coil).

In this context the, CALICE collaboration [5] developed several high segmentation calorimeters. The examples of the active media of these calorimeters are scintillators of the Analog Hadron Calorimeter (AHCAL) and the Scintillator Tungsten (ScW) Electromagnetic Calorimeter; Silicon of the Silicon Tungsten (SiW) Electromagnetic Calorimeter; Resistive Plate Chambers (RPCs) of the Digital and Semi-Digital Hadron Calorimeters (DHCAL and SDHCAL) as well as Monolithic Active Pixel Sensors (MAPS), Gas Electron Multipliers (GEMs) and Micromegas. The common point in these calorimeters is that they have high lateral and longitudinal segmentation. As a result, these calorimeters produce very nice pictures of particle interactions with unprecedented spatial resolution. For this reason, these calorimeters are often referred to as Imaging Calorimeters.

Here we report on special tests performed in the Fermilab test beam using the detector cassettes of the Digital Hadron Calorimeter prototype, the DHCAL [6], without absorber material interleaved between the active layers [7]. In this

Manuscript received on November 30, 2016.

Burak Bilki is with Beykent University, Istanbul, Turkey and the University of Iowa, Iowa City, IA, USA, e-mail: Burak.Bilki@cern.ch.

Benjamin Freund is with McGill University, Montréal, Canada, e-mail: freundb@physics.mcgill.ca.

José Repond is with Argonne National Laboratory, Argonne, IL, USA, e-mail: repond@anl.gov.

configuration, the so-called Min-DHCAL provided the opportunity to study electromagnetic and hadronic interactions with extremely fine segmentation. Furthermore, the electromagnetic interactions were imaged with a spatial magnification factor of around 5000 compared to the interactions in conventional electromagnetic calorimeters.

II. DESCRIPTION OF THE DHCAL WITH MINIMAL ABSORBER

The DHCAL used Resistive Plate Chambers (RPCs) [8] as active elements. The area of each RPC measured $32 \times 96 \text{ cm}^2$. The chambers utilized the traditional two resistive-plate design with soda-lime glass as resistive plates [9]. The cathode and anode plates were 1.15 and 0.85 mm thick, respectively, and enclosed a single 1.15 mm thick gas gap provided by fishing lines. The chambers were flushed with a non-flammable mixture of three gases: tetrafluoroethane (94.5%), isobutane (5.0%) and sulfur hexafluoride (0.5%). They were operated in avalanche mode with a default high voltage of 6.3 kV. Figure 1 shows a sketch of the RPC design.

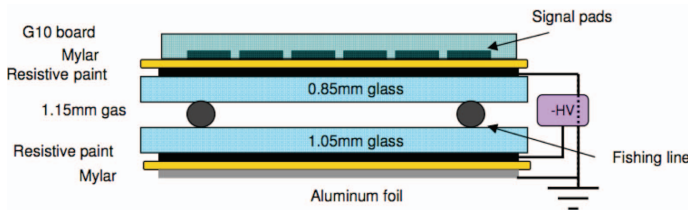


Fig. 1. Sketch of the DHCAL RPC design.

The readout boards each measured $32 \times 48 \text{ cm}^2$, contained 1,536 $1 \times 1 \text{ cm}^2$ pads, and were coupled to the anode plates. Two boards covered the area of one chamber. The readout boards contained two separate boards, the pad board and the front-end board, interconnected by dots of conductive glue. The electronic readout system was based on the DCAL III chip [10], which applies a single threshold to the signals from an array of 8×8 readout pads to define hits [6], hence ‘digital’ readout. The threshold discriminating the signals can be set individually for each DCAL chip and is common to all 64 channels connected to a chip. The readout is pulsed with a 10 MHz clock. After receipt of an external trigger, hit patterns of the 64 channels connected to a chip and in seven consecutive 100 ns time bins are read out together with their corresponding time stamps.

In order to hold in position and protect the three RPCs in a given layer and their six readout boards for both transportation to and insertion into the absorber structure, a cassette design was developed. The front-plate consists of 2 mm steel, while the back-plate is made of 2 mm copper. The latter is in contact with the front-end ASICs of the readout boards and serves to dissipate the heat generated by the electronics. Figure 2 shows the photograph of a cassette before the copper plate is mounted.

The Min-DHCAL consisted of 50 cassettes, spaced every 2.54 cm. The thickness of the entire stack corresponded to approximately $15 X_0$ or $1.7 \lambda_I$ with the thickness of each

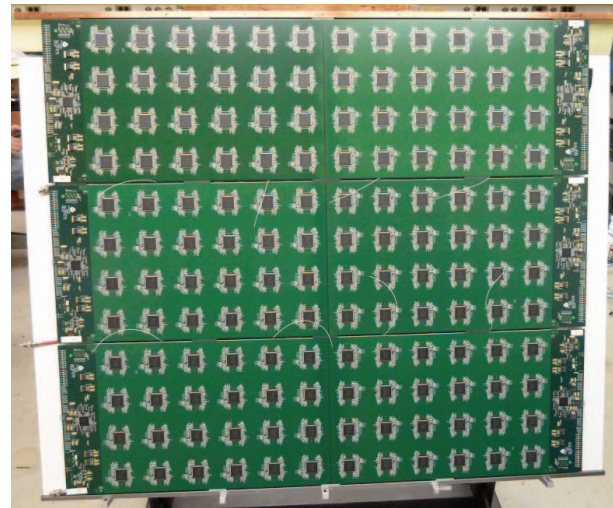


Fig. 2. Picture of a semi-assembled cassette without the copper plate.

layer corresponding approximately to $0.29 X_0$ or $0.034 \lambda_I$. The total number of readout channels was 460,800, which at the time constituted a world record for calorimetry in High Energy Physics. Figure 3 shows a photograph of the Min-DHCAL.

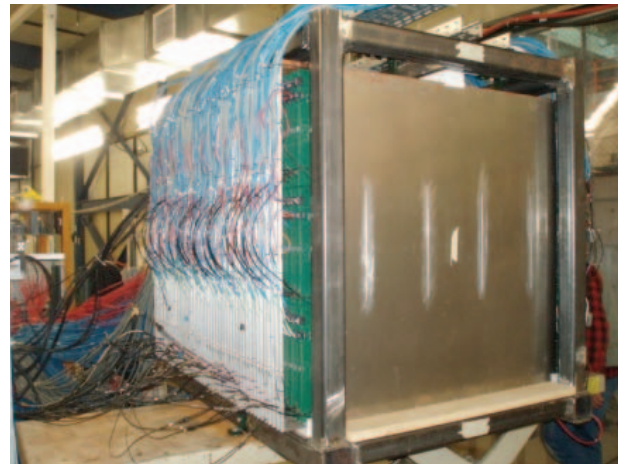


Fig. 3. Picture of the Min-DHCAL.

III. EXPERIMENTAL MEASUREMENTS AND SIMULATIONS

The Min-DHCAL was exposed to the test beam at the Fermilab Test Beam Facility, FTBF [11]. The data on which this paper is based were collected in November 2011. Runs were taken with a selected momentum in the range of 1 - 10 GeV/c. The beam was a mixture of electrons, muons and pions, where the fraction of electrons is dominant at momenta below 5 GeV/c and tapers off for momenta above 32 GeV/c. The beamline included two Čerenkov counters for particle identification and two scintillator paddles ($19 \times 19 \text{ cm}^2$), located approximately two meters upstream of the Min-DHCAL. The data acquisition was triggered by the coincidence of these two paddles. The discriminated signal

of the Čerenkov counters were read into the data stream and used offline to separate positrons from muons and pions. Approximately 800,000 triggered events were collected with the Min-DHCAL.

The simulation of the test beam set-up is based on the GEANT4 version 10.02 with default parameters [12]. The simulated set-up includes the active elements with their cassette covers, resistive plates, gas gap, and the electronic readout boards, in addition to the material in the beam line upstream of the stack. Any energy deposition generated by the simulation in the gas gap of the RPCs is used as a seed for creating an avalanche.

The response of the RPCs is simulated using a standalone program, called RPC_sim [13]. RPC_sim generates a charge according to measurements of the avalanche charge distribution, spreads the charge onto the anode plane and defines hits in pads by applying a threshold on the charge. The generated charge is spread over the anode plane assuming a drop-off with distance from the center of the avalanche described by the sum of two one-dimensional Gaussians. The charges induced by different avalanches on a given pad are summed up. A threshold is applied on the summed-up charge to define a hit.

Initially, the GEANT4 program utilized the FTFP_BERT physics list. However, this led to a unsatisfactory description of, among other measurements, the energy resolution, suggesting the generation of too few initial ionizations in the gas gap of the RPCs. A migration to the Option 3 or ‘_EMY’ based electromagnetic physics list, which is particularly appropriate for low energies and has an improved multiple scattering modeling, resulted in a significant improvement of the description of the experimental data. In the following, unless noted otherwise, the results of the simulation are based on FTFP_BERT_EMY physics list.

A number of event selection criteria was applied to the data and simulation:

- Only the hits within a 200 ns gate i.e. two time bins are considered (applied only to data).
- The hits in each layer of the DHCAL were clustered using a simple nearest-neighbor clustering algorithm. Two hits were assigned to the same cluster if they shared a common side. Events containing multiple particles and showers which initiated upstream of the DHCAL were suppressed by requiring a single cluster of hits with a maximum of four hits in the first layer of the stack.
- At least six active layers are required.
- Čerenkov counter signal above the positron threshold is required (applied only to data).

On the average 98 % of the simulated events passed the selection criteria. This fraction varies from 60 % at 1 GeV to 30 % at 10 GeV for the data as the fraction of the positrons in the mixed beam depends on the beam momentum.

IV. MIN-DHCAL RESPONSE TO POSITRONS

Through-going muon tracks are used to measure and equalize the response of the 150 different RPCs in the stack. The calibration factor C_i for chamber i is calculated as the product of the efficiency ε and pad multiplicity μ averaged over the

entire stack, divided by the same product as determined for chamber i . The efficiency ε for detecting a minimum ionizing particle is calculated as the ratio of tracks producing at least one hit to the total number of tracks crossing a given chamber. The average pad multiplicity μ is determined as the average number of hits for tracks which generate at least one hit in that chamber. For the Min-DHCAL, the average values were 0.917 for the efficiency and 1.573 for the pad multiplicity.

Figure 4 shows the distributions of the total number of hits for the Min-DHCAL both for data (top) and the simulation (bottom). The response curves have been normalized to unity for each momentum selection and are well described by fits to a Gaussian function in the range of $\pm 2\sigma$ around the peak value.

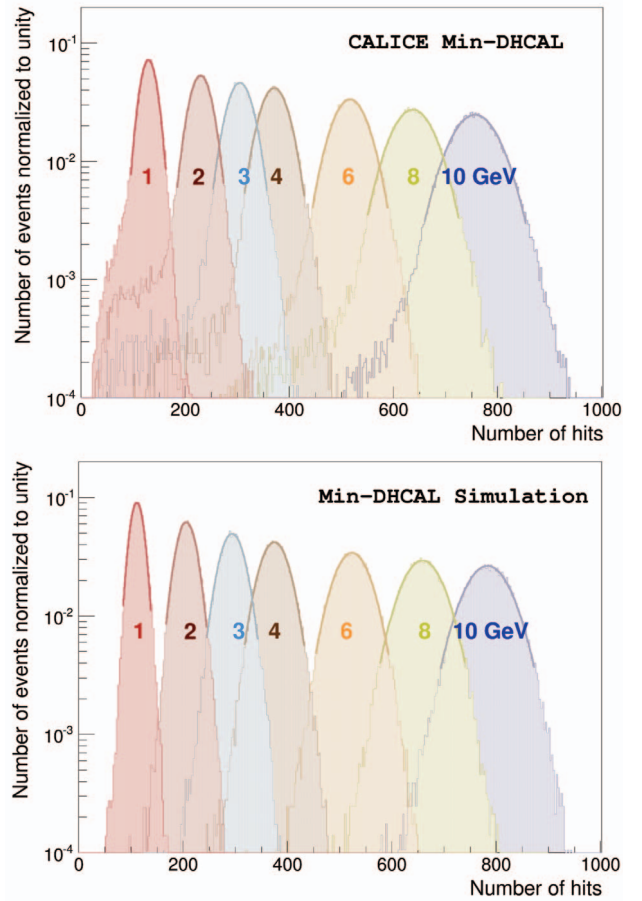


Fig. 4. Distributions of the total number of hits for data (top) and the simulation (bottom).

The mean values obtained from the Gaussian fits are shown as function of beam energy in Fig. 5. The statistical error is smaller than the size of the points. The systematic error is dominated by contributions from the calibration uncertainty. The data (red) are compared to the results of the Monte Carlo simulation based on both the FTFP_BERT (black) and the FTFP_BERT_EMY (blue) physics lists. Both are seen to be in good agreement with the data. The data/simulation are fit to a power law $N_{hit} = a(E_{beam}/GeV)^m$ where the exponent m is a measure of the non-linearity (saturation) of the response. A value of unity would indicate a perfectly linear response. A

value of $m = 0.76 \pm 0.02$ (0.836 ± 0.001) is obtained for data (simulation based on FTFP_BERT_EMY), indicating a strong saturation of the response. The saturation is mostly due to the large pad size compared to the density of particles in the core of electromagnetic showers. The observed difference between data and simulation is due to a trend of the simulation to feature less hits at low energy and more hits at higher energy compared to the measurements. The simulation based on the FTFP_BERT physics list produces similar results as the ones based on FTFP_BERT_EMY.

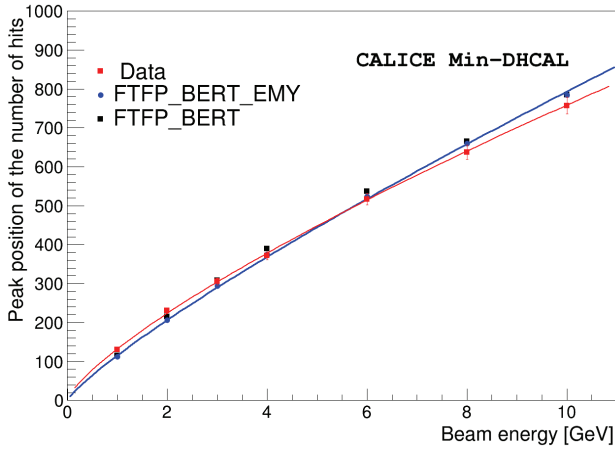


Fig. 5. Peak position of the number of hits versus positron beam energy for both data (red) and simulation based on FTFP_BERT (black) and FTFP_BERT_EMY (blue).

The obtained non-linear relation is then used to reconstruct the energy on an event-by-event basis. The reconstructed energy spectra are used to calculate the energy resolution. Figure 6 shows the electromagnetic energy resolution both for data and simulation. The measured widths are approximately 15% better than the corresponding resolutions obtained by the simulation based on the FTFP_BERT physics list, indicating a possible deficit in the number of ionizations in the gas gap. On the other hand, the simulation based on the FTFP_BERT_EMY physics list reproduces the measurements quite well, but are in average about 6% better than the data. The energy resolution versus beam energy was fitted to the standard parametrization with a stochastic and a constant term $\sigma/E = \alpha/\sqrt{E} \oplus c$. The stochastic term obtained for the data (simulation with FTFP_BERT_EMY) is 14.3 ± 0.4 (13.4 ± 0.2) and the constant term is 6.3 ± 0.2 (6.2 ± 0.1).

V. MEASUREMENT OF ELECTROMAGNETIC SHOWER SHAPES

The spatial segmentation of the DHCAL provides an unprecedented tool for the detailed study of the shape of electromagnetic showers. The measurements in the present configuration with minimal absorber material spread electromagnetic showers over the entire depth of the Min-DHCAL stack (approximately 1 m x 1 m x 1.3 m). This by itself means that the electromagnetic shower images are magnified by a factor of around 5000 compared to the conventional

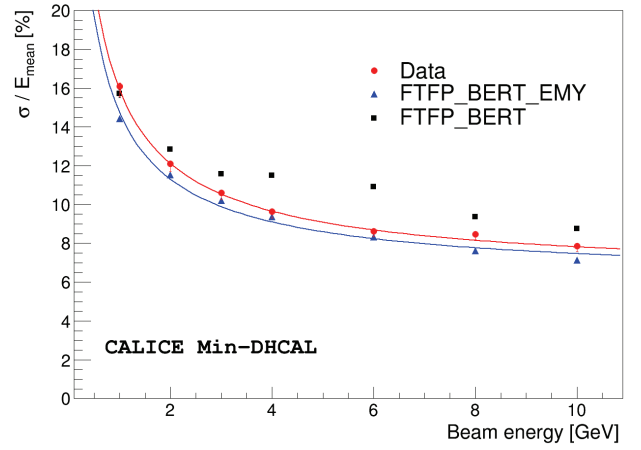


Fig. 6. Energy resolution versus positron beam energy for data (red) and simulation based on FTFP_BERT (black) and FTFP_BERT_EMY (blue).

electromagnetic calorimeters. Figure 7 shows the event display of an 8 GeV positron shower.

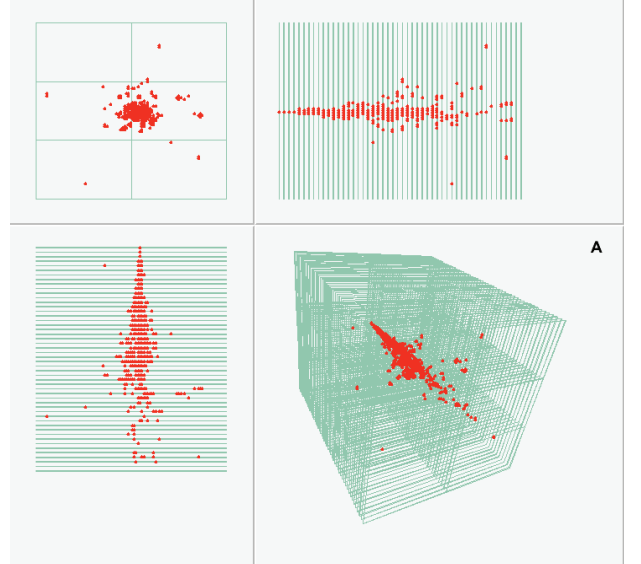


Fig. 7. Display of an electromagnetic shower measured in the DHCAL and initiated by an 8 GeV positron. Starting from the upper left and going clockwise the views are: x/y , x/z , $x/y/z$, and y/z , where x is horizontal and perpendicular to the beam, y is vertical and z is in the beam direction. The axes correspond to a right-handed coordinate system.

As an example of the longitudinal shower shape, Fig. 8 shows the average shape measured with 6 GeV positrons. The shower shape obtained with the simulation (blue histogram) shows reasonable agreement. The shower maximum is observed around layer 20, where the data exhibit a slight deficiency compared to the simulation. This discrepancy does not seem to originate from the limited rate capability of the RPCs, as selecting events in the first half second of each spill result in the same depletion at shower maximum. The difference can stem in part from the non-perfect equalization procedure of the RPC response.

The hit positions in the first five layers are fit to a line to obtain the trajectory. The transverse development of the

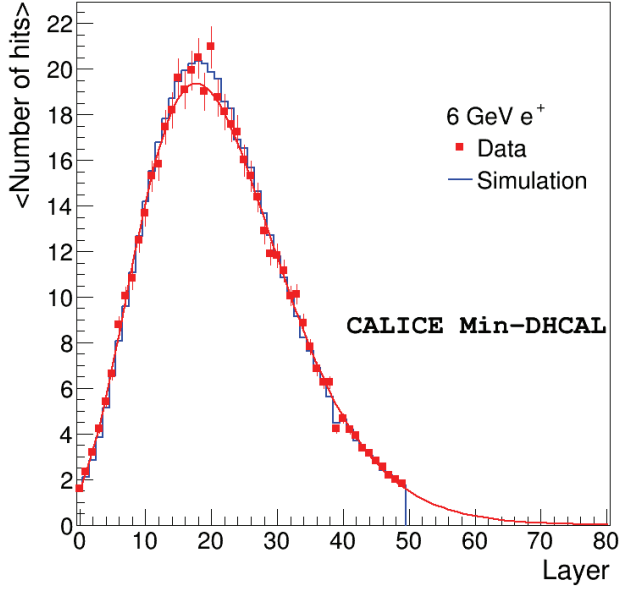


Fig. 8. Longitudinal shower shape for 6 GeV positrons.

electromagnetic showers is calculated with respect to this trajectory. As an example of the transverse shower shape, Fig. 9 shows the radial distance of each hit to the fitted straight line intersecting the corresponding detector plane, as measured for 6 GeV positrons. The accelerated decrease in entries above a radius of 50 cm is an artefact of the square shape of the detector planes with dimensions of 96 x 96 cm². Satisfactory agreement between data and simulation is observed over the entire range of radii apart from a small depletion at small radii in the data. Note that the number of hits varies over six orders of magnitude over the entire range in radii. Both the statistical and systematic uncertainties of the data are very small and mostly invisible in the plots.

The radial dispersion of hits in an event D_r is defined as:

$$D_r = \sqrt{\frac{R_i^2}{N} - \left(\frac{\sum R_i}{N}\right)^2} \quad (1)$$

where R_i is the radial distance of each hit to the trajectory. Figure 10 shows the average radial dispersion as a function of beam energy. For lower energies the data show larger radial dispersion compared to the simulation.

The density of hits is defined for each hit in an event as the number of hits in a volume of 3 x 3 x 3 pads surrounding the hit and can range from 0 to 26. Figure 11 shows the distribution of the density of hits for 6 GeV positrons for both data (red) and simulation (blue). The simulation shows a higher probability for higher hit densities than the data. The isolated hits observed in the data are not compatible with noise as the average number of accidental noise hits was measured to be ~ 0.2 in a reconstructed event. These hits are part of the electromagnetic shower and the simulation cannot reproduce them effectively. This indicates a still persistent lack of multiple scattering modeling in the simulation.

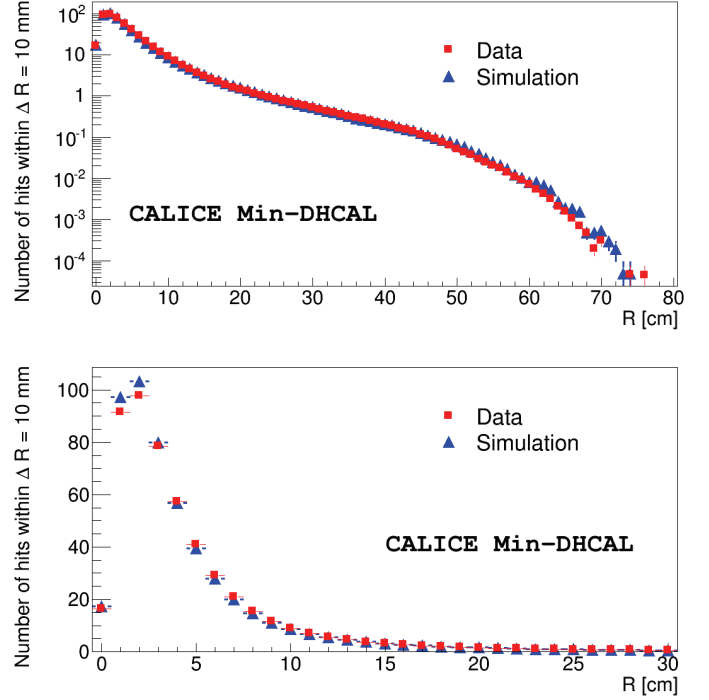


Fig. 9. Distribution of the radial distance of hits from shower axis for 6 GeV positrons. The upper (lower) plot uses a logarithm (linear) y-scale.

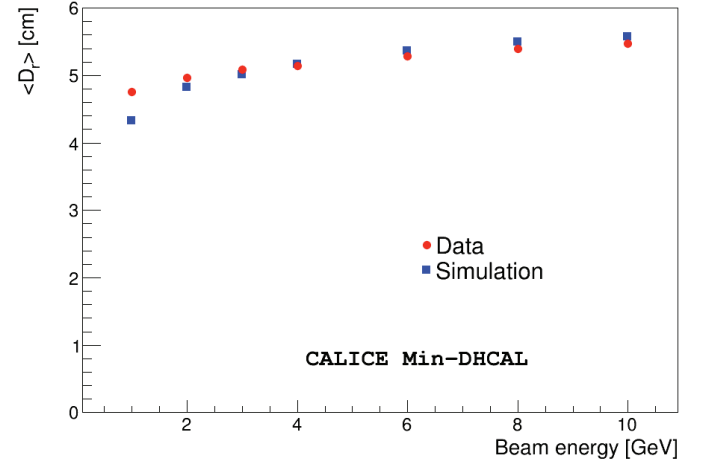


Fig. 10. Radial dispersion of hits in an event versus beam energy: data (red) and simulation (blue).

VI. LINEARIZATION OF THE MIN-DHCAL RESPONSE

The high spatial segmentation of the imaging calorimeters allow the application of corrections to the measured number of hits which might result in an improved linearity of the response and energy resolution.

In order to estimate the contribution of leakage out of the back of the calorimeter to the response to positrons, the fit functions to the measured longitudinal shower shapes were extended beyond the actual depth of the DHCAL, as shown in Fig. 8 [7]. Integration of the curves provides an estimate of the effect of leakage.

Next, in an attempt to improve the energy resolution for

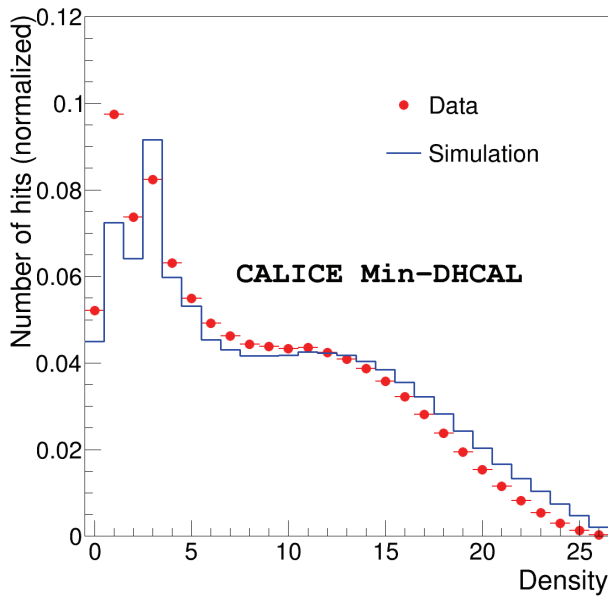


Fig. 11. Distribution of the density of hits in events induced by 6 GeV positrons: data (red) and simulation (blue).

positrons, the hits from a subsample of events recorded at each of the seven energy points were weighted depending on their hit densities. The details of obtaining the weights are given in [7]. The larger values of the weights related to higher hit densities compensate for the saturation effects introduced by the high density of electromagnetic showers and the finite pad size of the readout boards.

Figure 12 shows the response (peak position of the number of hits) as a function of beam energy before any corrections (blue), after leakage correction (red) and after linearization (green). The m values of the fits to the power law (see Section IV) are 0.78 ± 0.02 after leakage corrections and 0.94 ± 0.01 after linearization procedure.

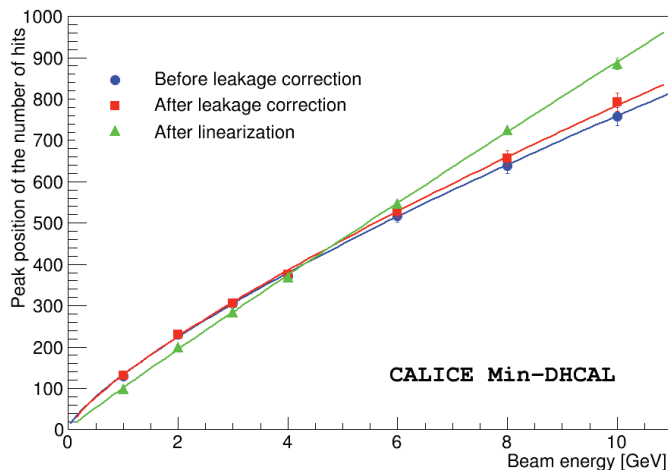


Fig. 12. Measured peak position of the number of hits for positrons as a function of beam energy: before any correction (blue), after leakage corrections (red) and after linearization of the response based on the hit densities (green).

Figure 13 shows the energy resolution as a function of beam energy obtained both before (blue) and after (red) the linearization procedure. The points have been corrected for the contribution from the known momentum spread of the test beam. The density-weighted linearization procedure results in a modest improvement of about 10 %. The stochastic term obtained after the linearization procedure is 13.0 ± 0.4 .

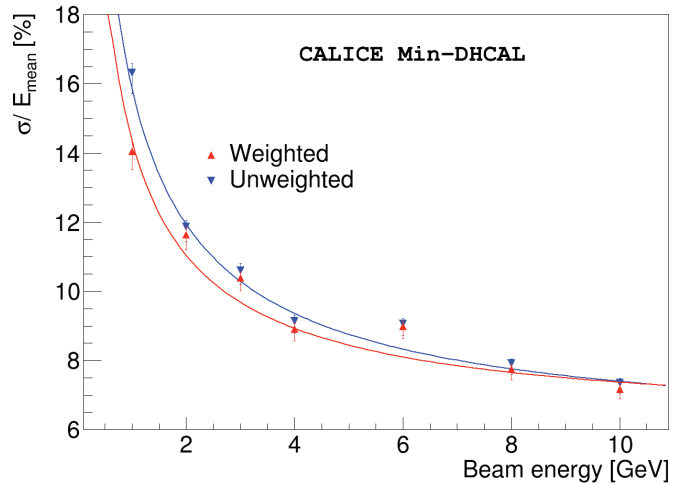


Fig. 13. Energy resolution versus beam energy for positrons: before (blue) and after (red) the linearization procedure.

VII. CONCLUSIONS

The CALICE Digital Hadron Calorimeter (DHCAL) detector planes without absorber plates, the so-called Min-DHCAL, was exposed to particles in the Fermilab test beam. The response of the Min-DHCAL to positrons, its energy resolution and various electromagnetic shower shapes were measured in the energy range of 1 to 10 GeV. The fine segmentation allows the study of electromagnetic showers with unprecedented level of spatial detail.

The results of a Monte Carlo simulation based on GEANT4 and a standalone program, RPC_sim, to emulate the response of the RPCs, were compared to the data. The GEANT4 simulation utilized both the FTFP_BERT and the FTFP_BERT_EMY physics lists and it was observed that the latter provides higher accuracy, in particular for the simulation of electromagnetic processes in thin layers.

REFERENCES

- [1] <https://www.linearcollider.org/ILC>
- [2] <http://clic-study.web.cern.ch/>
- [3] <https://fcc.web.cern.ch/Pages/default.aspx>
- [4] C. Adloff, et al., JINST 6, P07005, 2011.
- [5] <https://twiki.cern.ch/twiki/bin/view/CALICE/WebHome>
- [6] C. Adams, et al., JINST 11, P07007, 2016.
- [7] B. Freund, et al., JINST 11, P05008, 2016.
- [8] R. Santonico, et al., Nucl. Instrum. and Meth. 187, 377-380, 1981.
- [9] G. Drake et al., Nucl. Instrum. and Meth. A578, 88 - 97, 2007.
- [10] A. Bambaugh et al., Nuclear Science Symposium and Medical Imaging Conference (NSS/MIC), 2011 IEEE; DOI: 10.1109/NSS-MIC.2011.6154437.
- [11] <http://www-ppd.fnal.gov/ftbf/>
- [12] S. Agostinelli et al., Nucl. Instrum. Methods A506, 250 (2003).
- [13] B. Bilki et al., JINST 4 P04006 (2009).